Theoretical and Applied Climatology (2020) 139:861–872
https://doi.org/10.1007/s00704-019-03000-w

ORIGINAL PAPER

Systematic precipitation redistribution following a strong hurricane landfall

Paul W. Miller[1] · Thomas L. Mote[2] · Abhishek Kumar[2] · Deepak R. Mishra[2]

Received: 12 February 2019 / Accepted: 11 September 2019 / Published online: 7 November 2019

Abstract

The 2017 and 2018 Atlantic hurricane seasons poignantly illustrated the dangers tropical cyclones pose to US, Central American, and Caribbean coastlines. In particular, Hurricane Maria inflicted widespread damage, including catastrophic defoliation, to Puerto Rico, altering surface heat fluxes and possibly modifying precipitation patterns. This study assesses whether defoliation-driven changes to surface energy fluxes redistribute precipitation in the months following a powerful hurricane landfall. Remote sensing analyses of Maria-related vegetation reduction and recovery from Puerto Rico were adapted to the Georgia coastline. In this novel methodology, the resulting landscape evolution, characterized by an instantaneous vegetation reduction with a gradual recovery, was assimilated into the Weather Research and Forecasting model at a convection-allowing a 3-km grid spacing for the 1 June–1 August 2017 period. The experiment revealed that Maria-scale defoliation reduced precipitation by 14% during the month following landfall within a 50 × 50 km zone containing the hypothetical landfall location. A maximum deficit of 20.0% was reached 4 weeks after landfall. For June 2017, the modeled 14% deficit would have shifted the precipitation total from the 61st to the 47th percentile for years 1981–2016. Meanwhile, precipitation totals were unchanged on the domain scale. The near-landfall drying was also evident in three less-severe defoliation simulations, suggesting that systematic precipitation redistribution near the landfall location is possible following storms considerably weaker than Hurricane Maria. Analyses of the temperature and wind fields suggest that coastal kinematic flow is altered by the introduction of a thermally driven pressure gradient in the defoliated zone.

1 Introduction

The active 2017 and 2018 Atlantic hurricane seasons underscored the danger that tropical cyclones pose to inhabitants of the Caribbean, Central American, and US coastlines. In particular, the impact of Hurricane Maria on the island of Puerto Rico poignantly illustrated the devastating consequences of sustained high winds on the natural and built environments. Although the powerful winds, heavy rain, and storm surge responsible for the primary devastation waned as the hurricane departed the island, the landscape modification inflicted by the storm did not. Following widespread defoliation, reduction in plant transpiration leads to changes in evapotranspiration (ET) and latent and sensible heat fluxes, with the sign of the change depending on available soil moisture (Barr et al. 2012). The redistribution of heat fluxes may modify regional precipitation patterns, resulting in dry or wet spells that further inhibit recovery efforts. Thus, hurricanes may also initiate longer-lasting, secondary meteorological impacts via landscape modification.

A recent study of persistent hydrological consequences of Hurricane Maria in Puerto Rico noted that the post-landfall defoliated period was characterized by a statistically significant shift in the relationship between regional cloud cover and the atmosphere's thermodynamic structure (Miller et al. 2019). During the period of suppressed ET, the atmosphere's thermodynamic state (i.e., heat and moisture content) explained substantially more variation in daily cloud area, suggesting that land-atmosphere interactions were muted in the absence of the thick forest canopy.

Systematic precipitation redistribution is not a purely hypothetical outcome. Modeling experiments have shown that circulations caused by sensible heat flux variations can drive

✉ Paul W. Miller
pmiller1@lsu.edu

[1] Department of Oceanography and Coastal Sciences, Louisiana State University, Baton Rouge, LA 70803, USA

[2] Department of Geography, University of Georgia, Athens, GA, USA

regional precipitation patterns in Texas (Hu et al. 2017), and that forest mortality in the Rocky Mountain headwaters can significantly modify the surface energy budget (Forrester et al. 2018). Following Hurricane Hugo (1989) in Puerto Rico, physical scientists working in the eastern mountains noted a 400-m increase in the altitude of the orographic cloud layer and a 3-month dry spell (Scatena and Larsen 1991). In addition to the primary ecological consequences caused by the slope failures and Hugo's winds, secondary consequences associated with the 3-month dry spell were noted via animal populations (Woolbright 1991) and fine root mortality (Parrotta and Lodge 1991). The sequence of physical processes leading to the drying and ecological damage are generalizable beyond Puerto Rico.

The purpose of this study is to determine whether hurricane-related defoliation can lead to persistent hydrometeorological consequences in a coastal region. This study employs the Weather Research and Forecasting (WRF) model with an evolving land surface to simulate the instantaneous removal of vegetation followed by a gradual regrowth and recovery in regions with dominant woody vegetation. To our knowledge, this is the first time WRF is used to model vegetation-precipitation feedbacks following an acute wind disturbance. The findings of this work are valuable to water managers, emergency managers, and agricultural interests within afflicted regions. Because this research focuses on secondary hurricane impacts that persist after the largest perceived threats have passed, stakeholders likely do not currently account for them in preparation and recovery planning.

2 Methods

2.1 Study area

The modeling experiment is focused on coastal GA USA, denoted as GA in Fig. 1 along with other neighboring states in the Southeast USA. This region has been acknowledged for its vulnerability to hurricane hazards (Bossak et al. 2014). Though a hurricane has not made direct landfall on the Georgia coast since Hurricane David in 1979, the state recently experienced several tropical system interactions and near-misses. Hurricanes Matthew, Irma, and Michael each produced damaging winds and storm surge along the Georgia Atlantic coast in 2016, 2017, and 2018, respectively. In fact, Bossak et al. (2014) noted that Georgia's recent dearth of direct landfalls is not a historically consistent pattern. Between 1851 and 2012, fourteen hurricanes made landfall in coastal Georgia with the 1851–1900 witnessing nine such events.

Further, Georgia is susceptible to hurricane hazards from two directions. Though direct landfalls are only possible along the Georgia's Atlantic coast, the state also experiences acute

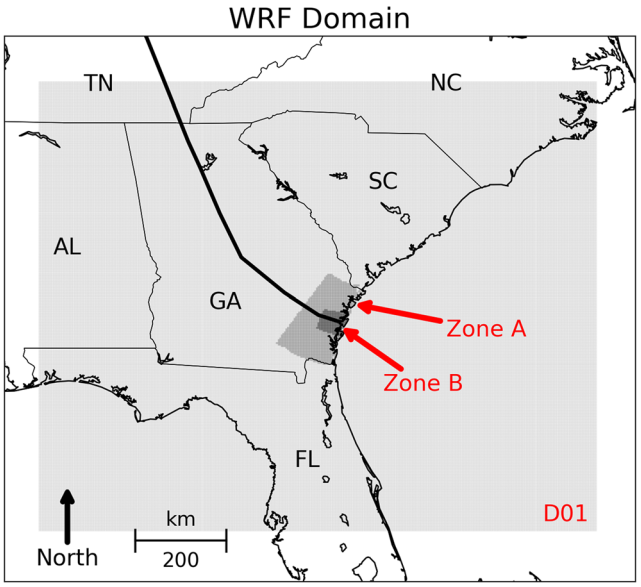

Fig. 1 WRF simulation domain (light gray, D01) with two near-landfall zones identified that are employed in the analysis. The hypothetical hurricane path is shown in black. Zone A represents all point within 100 cross-path km and 100 along-path km from the landfall, whereas Zone B contains points within 25 km cross-path and 50 km along-path

impacts from landfalling hurricanes along Florida's Gulf Coast. For instance, when Hurricane Michael struck the Florida panhandle and progressed northward in 2018, wind gusts as high as 115 mph were recorded in south Georgia (NWS 2018). Georgia economic losses from Hurricane Michael encompassed the following industries: forestry $762 million; cotton $550–600 million; pecans $560 million; vegetables $480 million; nurseries $13 million; poultry $25 million; peanut $10–20 million; soybeans $10–20 million (Georgia Department of Agriculture 2018a; Georgia Department of Agriculture 2018b). Because this study focuses on persistent hydrometeorological impacts of hurricanes, which are particularly relevant to agricultural interests, Georgia provides a suitable setting for the simulation.

2.2 Model initialization

This study employs WRF 3.8 (Skamarock and Klemp 2008) to discern the effect of hurricane-related defoliation on coastal hydrometeorology. WRF is often employed in regional climate modeling research and is routinely applied to test hypothetical effects of land-cover modifications (e.g., Shem and Shepherd 2009; Shepherd et al. 2010). By default, WRF is initialized using a static land surface based on the NLCD 2006 as well as remotely sensed land-surface radiative and vegetative properties. For longer climate simulations, the static land surface may be replaced with an intra-annually varying surface, which captures seasonal changes to sea surface temperatures and phenology from a remotely sensed climatology. However, in this case, the default land-surface characteristics

are overridden to test the consequences of hurricane-inflicted landscape modification on regional climate. Previous efforts have used WRF to simulate the spatial distribution of hurricane precipitation for altered land cover (Wang et al. 2016), while other efforts have implemented NASA Unified WRF (NU-WRF) to simulate landscape-precipitation feedbacks during longer-term disturbances, such as drought (Zaitchik et al. 2012). However, the authors cannot identify any attempts to simulate the near-instantaneous removal of vegetation followed by a gradual landscape recovery from an acute wind disturbance, as we perform herein. Though simulations were performed with WRF 3.8, the study adopted the same physics options that were introduced as the "CONUS" suite in WRF 3.9. This combination of parameterization schemes has been previously tested and has produced reasonable results (UCAR 2017). The physics schemes and initialization details are provided in Table 1.

Based on remote sensing analyses from Miller et al. (2019), which quantified post-Maria defoliation in Puerto Rico, a "worst-case scenario" was developed for coastal Georgia defoliation. Additionally, three less-severe defoliation scenarios were adapted from the Maria-based worst-case scenario, representing 25%, 50%, and 75% of the Maria-inferred defoliation from Puerto Rico. Though the biogeography of the two locations varies, the methodology below has been designed to minimize the influence of these differences. The Miller et al. (2019) pre- vs post-Maria analysis for Puerto Rico generated island-averaged green vegetation fraction (GVF) and leaf area index (LAI) time series for approximately 1 month before and 5 months following landfall. These time series were used to inform the magnitude of GVF and LAI reduction that could plausibly arise from an intense hurricane interaction as well as the rate of recovery during the ensuing months.

The defoliated zone's cross-path structure is informed by statistical relationships in Hu and Smith (2018) relating post-Maria NDVI reduction to Euclidean distance from path, whereas the along-path structure is guided by the HURDAT 2 dataset (Landsea and Franklin 2013), which characterizes the post-landfall weakening of storms therein. These two datasets were integrated to yield a hypothetical two-dimensional defoliation zone for the Georgia coastline with the 1898 Category-4 Georgia hurricane serving as the prototypical storm. For instance, the Hu and Smith (2018) NDVI-distance model predicted ~ 40% NDVI reduction at a point 20 km from Maria's path. However, after progressing 100 km inland, the HURDAT2 dataset indicated that the 1898 storm's peak wind was 75% of the landfall intensity. Thus, points 100 km along-path from the landfall and 20 km from the path center received a ~ 30% reduction in NDVI (i.e., $0.40 \times 0.75 = 0.30$). The NDVI-path distance linear regression model in Hu and Smith (2018) was adapted for GVF and LAI, the required WRF inputs.

Though the landscapes of Puerto Rico and coastal Georgia vary and by extension possibly their response to a strong wind event as well, the methodology implemented herein is designed to be robust to any differences. The immediate Georgia coastline is characterized by abundant salt marshes before transitioning to evergreen forest and cultivated cropland further inland. However, remote sensing analysis by Ghosh et al. (2016) revealed a ~ 40% reduction in vegetation fraction and LAI within Louisiana's salt marshes following Category-3 Hurricane Katrina (2005). Category-2 Hurricane Gustav (2008) also reduced vegetation fraction and LAI, though not as dramatically (Ghosh et al. 2016), supporting the implementation of the less-severe defoliation scenarios for coastal Georgia. Additionally, because GVF and LAI for Georgia are altered proportionally, any discrepancies between GVF and LAI magnitudes do not bias the results. Though alternative strategies for developing hypothetical defoliation surfaces may be suggested, the procedure above yielded a reasonable, empirically based scenario to assess the primary science question described in Section 1.

Table 1 WRF initialization and parameterization schemes

Setting	Scheme
Cumulus	–
Microphysics	Thompson
Boundary layer	Mellor-Yamada-Janjic TKE
Land surface model	Noah
Radiation	RRTMG
Initialization	NAM analysis
SST data	NAM analysis
Boundary conditions	NAM analysis
Horizontal grid	350 × 300
Vertical levels	40
Horizontal grid spacing	3 km

2.3 Experimental design

WRF is initialized using boundary conditions from the North American Mesoscale model (NAM) from 25 May through 1 August 2017 with the first week discarded as spin-up time. The NAM is a numerical weather model with a 12-km grid spacing, which allows for a single nest to run at a convection allowing a 3-km grid spacing. Figure 2 compares the total precipitation from the WRF control run using the settings in Table 1 to the same 1-month precipitation total from the Parameter-elevation Regressions on Independent Slopes Model (PRISM) dataset (Daly et al. 1994). By incorporating daily station data with climatological precipitation distribution, PRISM spatially regresses observed precipitation while accounting for several physiographic factors such as elevation and distance to coast. As a whole, WRF tends to over-predict rainfall within the domain (note different color scales in Fig.

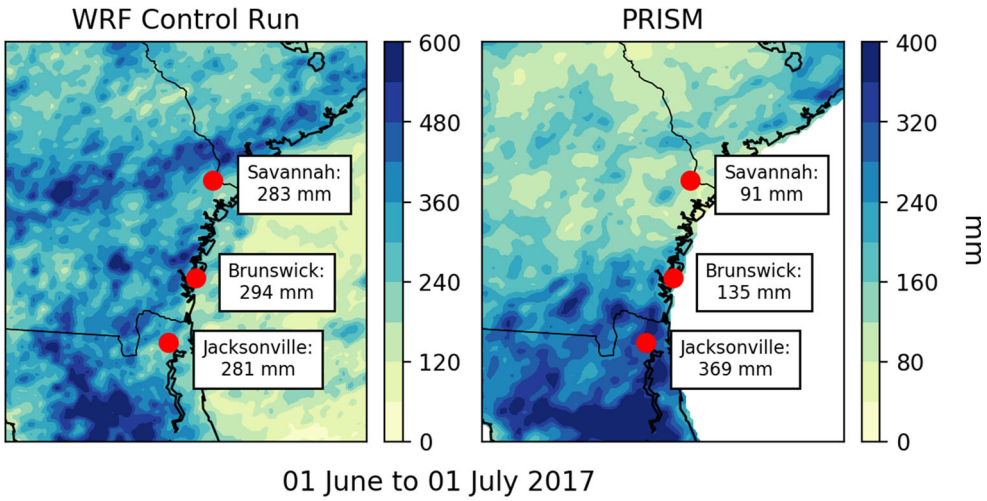

Fig. 2 Total precipitation generated by WRF control run between 1 June and 1 July 2017 compared to the PRISM analysis for the same time period. Note the different color scales between panes

2.), though this pattern varies spatially. For instance, WRF overestimated precipitation at Savannah/Hilton Head International Airport (KSAV) by 209%, whereas it underestimated precipitation at Jacksonville International Airport (KJAX) by 24%. WRF also over-emphasizes a precipitation band along a southwest to northeast corridor along the northern tier of Fig. 2. The preference for over-producing precipitation in convection-allowing WRF simulations has been reported in other studies as well, generally during the summer and afternoon convective periods (Pieri et al. 2015; Schwartz et al. 2009; Wang et al. 2018). However, because this study is a hypothetical event, it will focus solely on how the experimental defoliation simulations differed from the control.

A total of five WRF simulations were conducted: one control scenario (Fig. 2), the Maria-inferred defoliation scenario, and three intermediate scenarios representing 25%, 50%, and 75% of the Maria-inferred vegetation reduction (not shown). The NAM boundary conditions are identical for all five runs. Only the GVF and LAI fields are altered in the wrflowinput files. The 1-week spin-up period was conducted using the normal vegetation state, which was then substituted with the altered vegetation surfaces in Fig. 3 beginning on 1200 UTC 1 June 2017. In the control simulation, GVF and LAI vary slightly throughout the simulation consistent with the remotely sensed vegetation density increases throughout boreal summer. Though 1 June marks the beginning of hurricane season and is early for a Maria-strength storm, this date was selected to provide the greatest vegetation contrast during the experimental period. For instance, if the hypothetical landfall occurred in October, the hurricane-related defoliation would be less apparent because the landscape's deciduous trees may have already begun shedding leaf cover per the annual greening cycle. The analysis will primarily focus on differences between the control and Maria-like defoliation scenarios with the intermediate scenarios informing the tipping point at which precipitation impacts are manifested.

3 Results

3.1 Impact on surface energy budget

The impact of the hypothetical defoliation on the surface energy budget is illustrated in Fig. 3c–f. The defoliated zones shown in Fig. 3b are easily discerned when viewing the simulated latent heat flux fields (Fig. 3c) on 1 June and 15 June. Though cumulus activity near the coast may obscure the heat fluxes on some days, there is a decrease within the artificially defoliated region. Simultaneously, by restricting the ET potential of the land surface, the sensible heat flux (Fig. 3d) is correspondingly strengthened during the first few weeks of the simulation. As might be expected, the sensible (latent) heat flux increases (decreases) in proportion to the magnitude of defoliation. The Maria-equivalent defoliation scenario shows an initially dramatic increase (decrease) in sensible (latent) heat flux, which is still faintly discernible by mid-July. The modified moisture and energy transfers between the land surface and the boundary layer are manifested through both surface temperature and humidity. Minor 2-m temperature increases (Fig. 3e) and 2-m specific humidity decreases (Fig. 3f) are evident over the defoliated zone during early June but become indiscernible by July. Although the defoliation signature is visible in Fig. 3b through the end of the simulation, the impacts to the surface energy budget become marginal prior to the end of the simulation.

Table 2 characterizes changes in the areal mean of the aforementioned parameters within a 50 × 50 km area near the landfall (see Zone B in Fig. 1) during June and July 2017. Though changes to both the sensible and latent

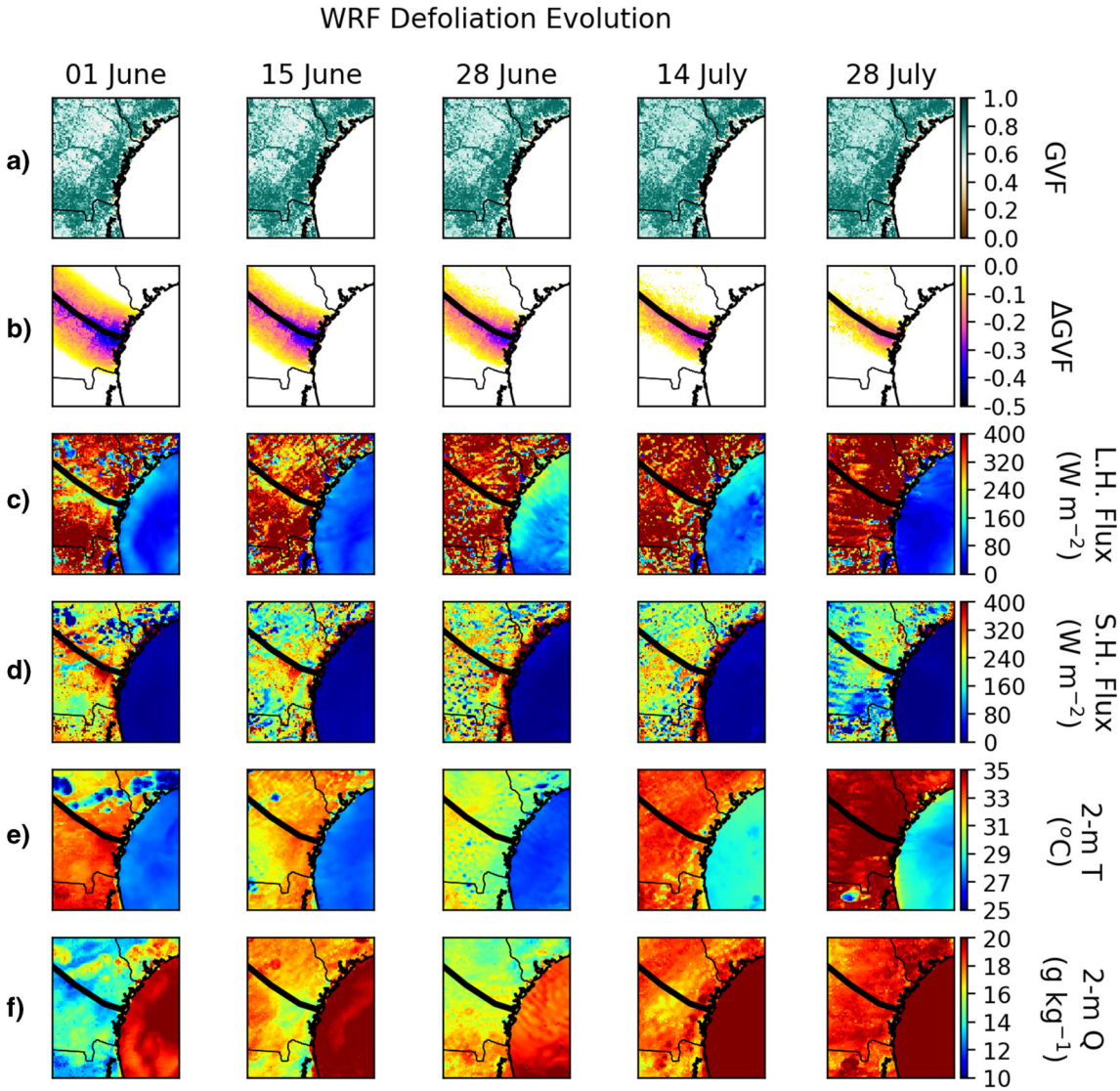

Fig. 3 (A) Green vegetation fraction (GVF) time series for the control and (B) Maria defoliation WRF simulations. The control time series displays the absolute GVF values, whereas the defolation scenario depicts the deviation from the control GVF. The WRF input surface recovers at a linear rate until the GVF reaches the control value. The (C) 1800-UTC latent heat flux shows clear decreases over the defoliated zone, whereas the (D) 1800-UTC sensible heat flux increases. Similarly, (E) 1800-UTC 2-m temperatures show subtle a increase, while (F) 1800-UTC 2-m specific humidities decrease. These changes are most dramatic 1 June and diminish as the vegetation recovers

Table 2 Differences in mean 1800-UTC atmospheric variables between June (30 days) and July 2017 (31 days) between the Maria defoliation scenario and the control simulation. Values represent areal means for locations within Zone B in Fig. 1. * indicates the experimental mean is significantly different from the control with 95% confidence as determined by a Student's *t* test

	June			July		
Scenario	Control	Maria defoliation	Percent difference	Control	Maria defoliation	Percent difference
Sensible H.F. (W m^{-2})	218	274*	26%	196	229*	17%
Latent H.F. (W m^{-2})	377	269*	− 29%	402	345*	− 14%
2-m T (°C)	29.8	30.4	2.0%	32.3	32.7	1.2%
2-m Q (g kg^{-1})	17.7	16.8	− 5.1%	18.5	18.0	− 2.7%

heat fluxes are statistically significant for both months, neither the 2-m specific humidity decrease nor the 2-m air temperature increase are statistically significant. However, the inland progression of the sea breeze by 1800 UTC each day may obscure potentially greater differences. The percent difference between the control and defoliation scenarios is greatest in June and wanes in July as the vegetation recovers, consistent with the visual progression of landscape recovery in Fig. 3.

3.2 Impact on precipitation totals

Figure 4 illustrates the net impact of these energy budget perturbations on the total precipitation between 1 June and 1 July 2017, when rainfall redistribution is most evident. Though the simulation was performed from 1 June to 1 August 2017, Fig. 3 and Table 2 show that changes to the surface energy fluxes, temperature, and specific humidity were most prominent during June, and indeed precipitation patterns during July showed marginal differences between the control and defoliation scenarios. On the domain-wide scale (Fig. 4a), there is essentially no difference in mean total precipitation between the defoliation simulation and the control on either the daily or monthly scale.

However, when the domain is narrowed to include only areas nearest to the landfall (see Zones A and B in Fig. 1), then differences in daily and 1-month totals emerge, generally reducing precipitation (Fig. 4b, c). The largest cumulative percent difference in Zones A and B (excluding the first 3 days during which cumulative percent differences are not meaningful due to small cumulative absolute precipitation totals) is 9.0% and 20.0%, respectively, with both occurring on 28 June 2017. A heavy rainfall event on 1 July 2017 ameliorates the Zone B deficit such that by 1 month after the defoliation, the rainfall shortfall decreases to 14%. Though not shown in Fig. 4, by the end of the 2-month simulation, the Zone A defoliated total is within 1% of the control. Similarly, by late July, the Zone B deficit has largely faded; however, a single event on 26 July 2017 re-intensifies the cumulative deficit to 15.3% a few days before the end of the simulation (not shown). Because the mean precipitation totals across the entire domain are effectively unchanged between the defoliation experiment and the control, the results in Table 2 and Fig. 4 imply that the modified heating patterns prompt a spatial *redistribution* of precipitation rather than wholesale suppression or enhancement.

When viewed spatially (Fig. 5), precipitation redistribution is evident during the 1-month period following the hypothetical landfall, suggesting that widespread defoliation can prompt hydrometeorological changes following a hurricane. However, there are no readily apparent patterns that might be logically attributed to the defoliation path. The band of higher precipitation totals spanning from southwest to northeast in the control simulation (Fig. 2) has been shifted, with positive anomalies abutting the zone to the north and south. Given the large variation in precipitation redistribution, attention is focused nearest the coast where changes to the surface energy budget were strongest (Fig. 3c–f), roughly corresponding to Zone A in Fig. 1. Immediately onshore and south of the defoliation path, there is a region of reduced rainfall with increased precipitation further north between the hypothetical landfall location and the Georgia (GA)-South Carolina (SC) border.

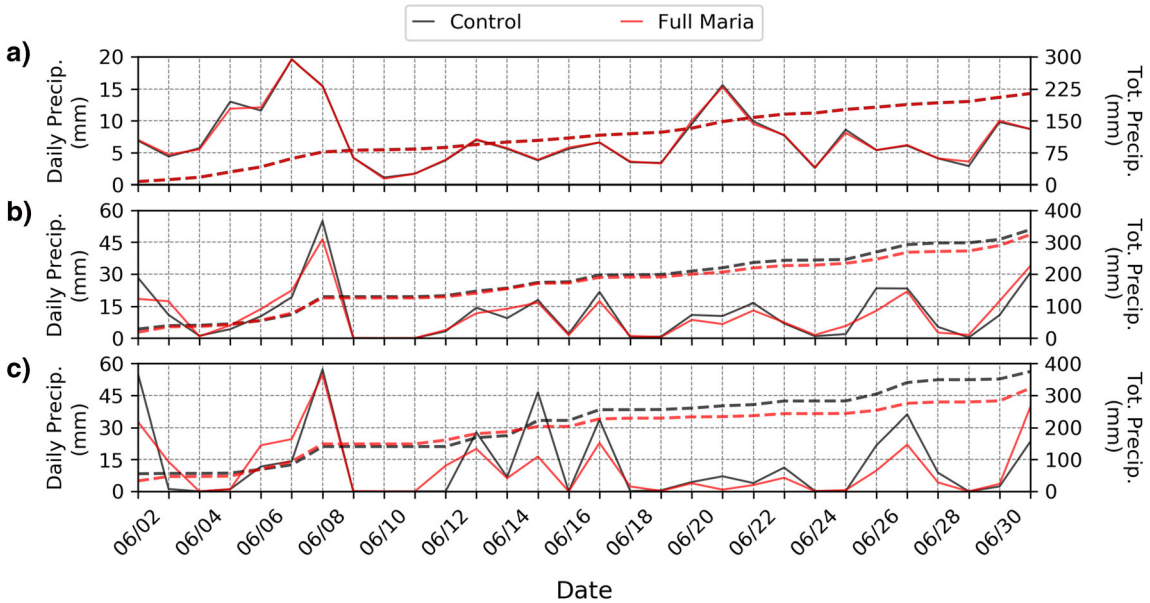

Fig. 4 Time series of daily (solid) and accumulated (dashed) precipitation for the two WRF scenarios. Area-averaged traces are shown separately for (A) the entire modelling domain, and the subset of the land surface within (B) Zone A and (C) Zone B shown in Fig. 1. Values for each date represent the amount of precipitation occurring during the 24-h period ending on 1200 UTC of the date listed

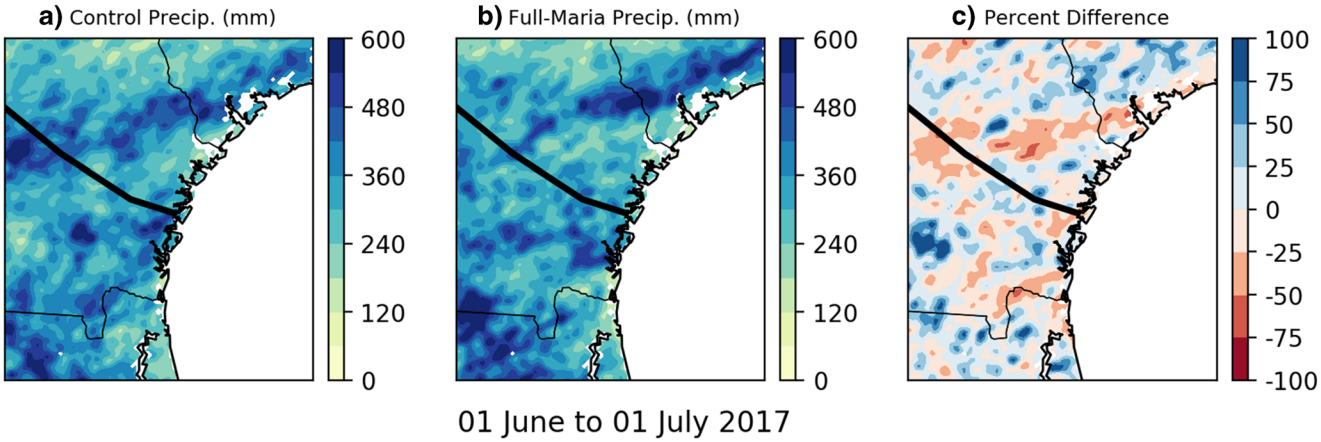

Fig. 5 Precipitation difference maps for the (**A**) control simulation compared to the Maria-like (**B**) defoliation scenario. (**C**) Percent differences (i.e., (Precipitation$_{Maria}$−Precipitation$_{Control}$)/Precipitation$_{Control}$] are calculated for the 1-month period from 1 June to 1 July 2017. The bold black line depicts the hypothetical hurricane center path

Due to the irregular geometry of enhanced/diminished precipitation areas in the defoliated scenario in the comparison map (Fig. 5), it was unclear whether the dry anomaly south of the track juxtaposed with increased precipitation to the north was a systematic or spurious result. Thus, the near-coastal precipitation differences for the three less-defoliated scenarios described in Section 2.3 were consulted (Fig. 6). All four defoliation scenarios show drying south of the landfall and moistening to its north although the contrast is paradoxically most apparent in the 25% defoliation scenario. Consequently, this outcome is judged to be a systematic, not spurious, consequence of the defoliation, and its underlying physical mechanisms will be analyzed further.

3.3 Physical mechanisms leading to systematic redistribution

By reducing the latent heat flux and enhancing the sensible heat flux, defoliation prompts conceptual changes to the boundary-layer thermodynamic composition by increasing 2-m temperature, creating thermally driven areas of decreased surface pressure, and perturbing kinematic flow near the coast. Figure 7 depicts changes to the coastal wind field on 15 June 2017, a day selected for its still-defoliated landscape (Fig. 3) and a quiescent synoptic pattern where local-scale processes would be more prominent. In addition, a 90-J kg^{-1} capping inversion in the 1200-UTC sounding from Jacksonville International Airport (see Fig. 2) on this day largely suppressed the formation of deep convective updrafts and outflows that confound changes to the regional energy budget and wind field on most other quiescent synoptic days. On 15 June 2017, the defoliation scenario is characterized by wind speed increases south of the center path and decreases to its north (Fig. 7a).

Further, temperature increases over the defoliated path also strengthen the land-sea temperature gradient driving the sea breeze circulation. At 1800 UTC on 15 June 2017, the sea breeze head is roughly 50% stronger than the control simulation along most of the Georgia coastline (Fig. 7a). In addition to stronger wind speeds, Fig. 7b illustrates modification to the wind direction as well. In the defoliated run, the onshore flow is oriented more orthogonal to the coast in addition to increasing in speed. The effect of the modified heating patterns on the sea breeze can be concisely communicated using the sea breeze index (SBI) developed by Frysinger et al. (2003) for Charleston, South Carolina. The SBI, shown in Eq. (1), is a ratio of the offshore synoptic wind speed (U) to the thermal potential energy related to the land-sea temperature contrast ($\Delta T = T_{air} - T_{sea}$), equipping it to characterize both thermodynamic and kinematic changes to the coastal environment with a single value. The +/− convention indicates that the original sign of U is applied to U^2 (+ for offshore; − for onshore), so that it is not lost when squared.

$$SBI = \pm\frac{U^2}{\Delta T} \tag{1}$$

The SBI was calculated using the SST immediately offshore of Brunswick, Georgia, and compared to the 2-m air temperature at a location 50 km inland from the coast. During the 61-day study period, 31 days possessed SBIs favorable for sea breeze formation, whereas this frequency modestly increased to 33 days in the defoliation scenario (though this was not a consistent result in the less-severe defoliation cases).

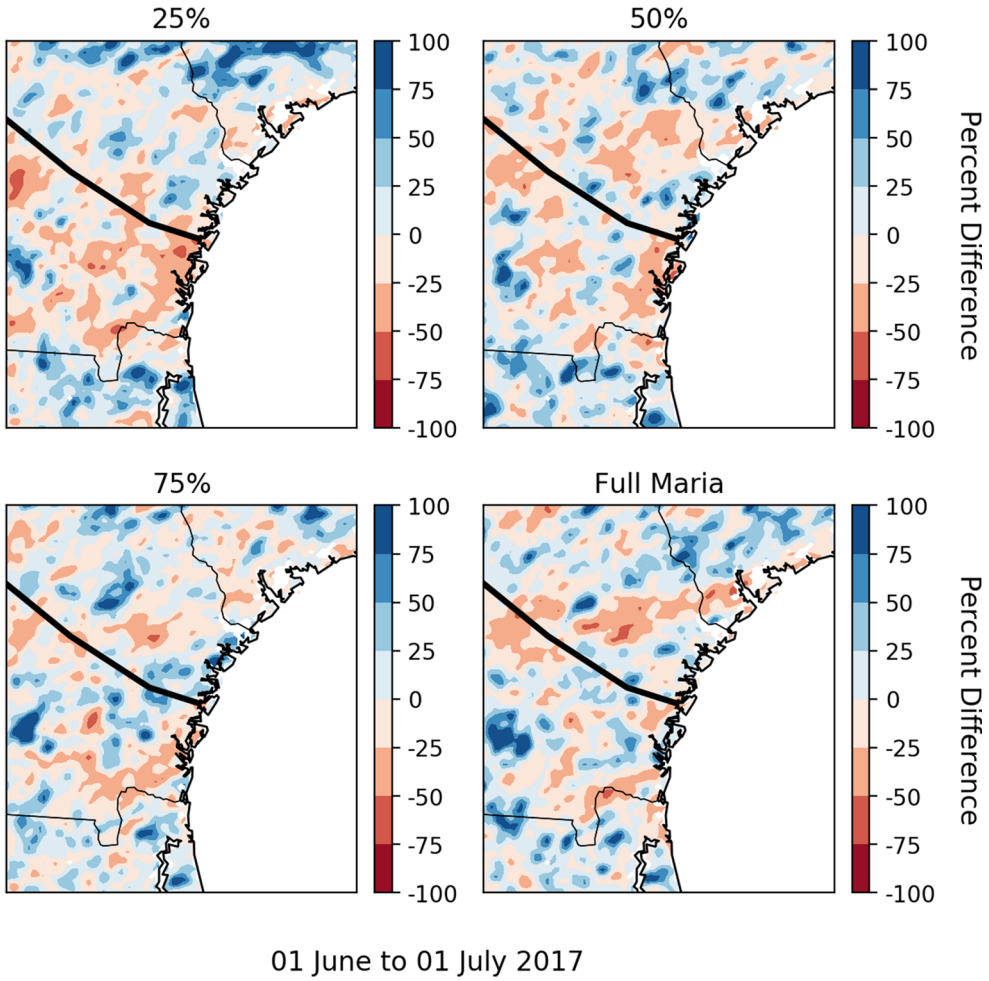

Fig. 6 Precipitation changes in all four defoliation scenarios compared to the control simulation. The bold black line depicts the hypothetical hurricane center path

Though Fig. 7 clearly indicates the consequence of defoliation on the sea breeze for 15 June 2017, the extent to which the altered energy budget consistently modified coastal kinematic circulations and thermodynamic environments is unclear. Because the study focused on longer-lasting (i.e., 30–60 days) hydrometeorological disruptions from hurricanes, the WRF analyses were written to disk in coarse 6-h intervals, yielding a single output field near peak diurnal heating. Frequently, active weather events were already ongoing at this time, obscuring the isolated modification resulting from the defoliation. For instance, the 1800-UTC output for the defoliated scenario on a particular day may show a 2-m air temperature reduction compared to the control. However, the reduction in temperature may be related to the displacement of

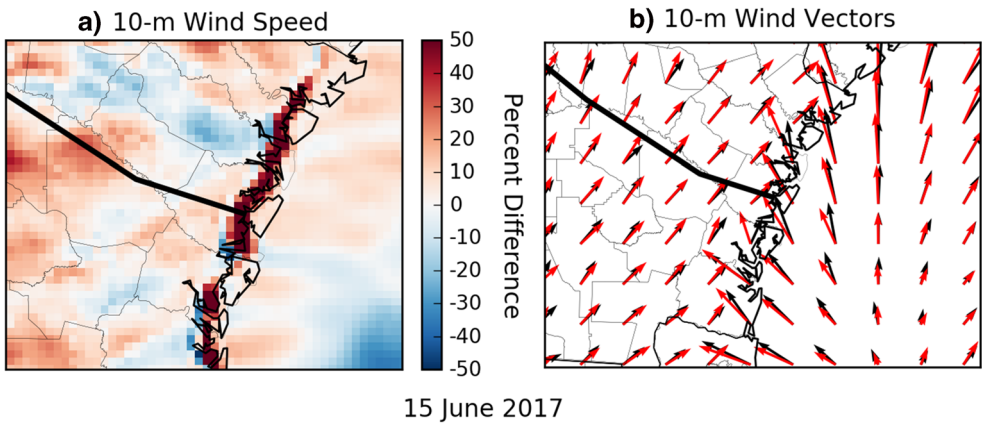

Fig. 7 Changes to the sea-breeze circulation on 15 June 2017 as characterized by (**A**) 10-m wind speed and (**B**) direction. The bold black line depicts the hypothetical hurricane center path. In (**B**), the red and black vectors correspond to the most severely defoliated and control simulations, respectively

thunderstorm activity that produced rain-cooled outflows over the hypothetical path. In such a case, the 2-m temperature may have shown an appreciable increase in the defoliated scenario prior to the thunderstorm, but no output was available at that time.

4 Discussion

The defoliated scenario in Fig. 4 ended the first month of the simulation with a 14% reduction in Zone B precipitation from the control run. For context, the PRISM analysis in Fig. 2 shows that the 1 June–1 July 2017 total precipitation for Brunswick, GA, was 135 mm compared to the 1981–2016 mean of 129 mm (https://xmacis.rcc-acis.org/), placing it in the 61st percentile for the 1981–2016 period. However, if the 135-mm total were to be reduced by 14% as in the defoliation scenario, then it would have fallen to the 47th percentile, making it a slightly below-average June. Whereas estimating the potential precipitation departures is valuable for water and emergency managers, meteorologists also need to understand the responsible physical processes to predict how future events may compare to the modeled scenario, benefitting decision-makers in turn.

In a thorough review paper describing vegetation-convection relationships, Pielke (2001) discusses how mesoscale vegetation changes can initiate changes in convective precipitation patterns that (1) affect scales much larger than the original disturbance and (2) are nonlinear. These two conclusions, reached by the sum findings of previous work, are manifested in the precipitation modification documented by this present study. For instance, vegetation reduction along the hurricane path is associated with large precipitation changes well beyond the disturbed landscape (Fig. 5). Similar work in the region performed by Sims and Raman (2016) showed that convection in the Carolina coastal plain was dependent on the interaction of the sea breeze and another circulation arising from differential heating over soil types. Thus, changes to the sea breeze circulation in Georgia may promote cascading effects that influence interactions with other boundary-layer fronts far away from the defoliated zone. Echoing the second Pielke (2001) theme, Fig. 6 illustrates the nonlinearity of the vegetation-precipitation relationship. In the 25% Maria defoliation scenario, the precipitation deficit upwind of the landfall location was greater than in the full defoliation run. Though the four progressively more severely defoliated simulations each predict roughly the same drying patch, the magnitude of the upwind deficit and downwind surplus is not commensurate to the magnitude of the hypothetical defoliation.

However, without greater temporal output resolution to firmly diagnose the physical processes leading to the precipitation redistribution (Figs. 5 and 6), we only hypothesize about changes occurring nearest to the coastline. In the near-coast region, defoliation was most severe, longest lasting, posed the clearest initial changes to the surface energy fluxes (Fig. 3c, d), and witnessed similar precipitation redistribution even in less-defoliated scenarios. In this respect, the first logical science question is "How would defoliation-driven thermal perturbations produce precipitation deficits upwind and surpluses downwind of the landfall under the prevailing synoptic wind direction?" [During the study period, 45% of all non-calm hourly wind observations at Jacksonville International Airport (see Fig. 2) possessed a southwesterly component (Midwestern Regional Cimate Center 2019).]

Figure 8 depicts a schematic hypothesizing an explanation for the reduction (enhancement) in wind speed occurring downwind (upwind) of the landfall on 15 June 2017 (Fig. 7a). When southwesterly synoptic winds prevail, the upwind zone experiences a like-oriented pressure gradient force related to the thermal contrast between the warmer defoliated zone and the cooler, fully vegetated landscape. This additional force enhances wind speeds upwind of the most severe defoliation. However, the thermally driven circulation opposes the synoptic flow in the downwind sector of the hypothetical path, retarding the synoptic flow. Figure 9 visualizes the planar superposition of the thermal circulation in Fig. 8 with the strengthened sea breeze front in Fig. 7b. Combining both outcomes, an enhanced convergence zone would form where the thermally reinforced synoptic wind field encounters the synoptically retarded flow and the strengthened sea breeze front (Fig. 9). This region of systematically preferred convergence is favorable for convection initiation; however, the prevailing southwesterly flow transports the deepening convection downstream where it deposits the greatest precipitation. For instance, according to the publicly accessible Plymouth State University upper-air analysis (http://vortex.plymouth.edu/myo/upa/raoblst-a.html), the storm motion vector inferred from the observed 0000-UTC Airport radiosonde wind profile from Jacksonville International Airport on 16 June 2017 was 238 degrees (i.e., nearly due southwest).

Though based largely on the 1800-UTC 15 June 2017 output for its still-diminished defoliation, quiescent synoptic regime, and absence of confounding thunderstorm outflows, the hypothesis stated above is supported by previous research. For instance, in a large eddy simulation, Rochetin et al. (2017) found that breezes arising from surface heat flux heterogeneities "induced a strong determinism" on the location of convection initiation. They also identified that the location of preferential triggering was a function of not only the breeze circulation but also how the breeze interacted with the background synoptic wind field. Similarly, Garcia-Carreras et al. (2010) found that "vegetation" breezes between crop and forest land in a tropical climate led to regions of enhanced convergence and convective development. Similar to our example on 15 June 2017, they noted that the effect of the vegetation breeze on convection initiation was insignificant

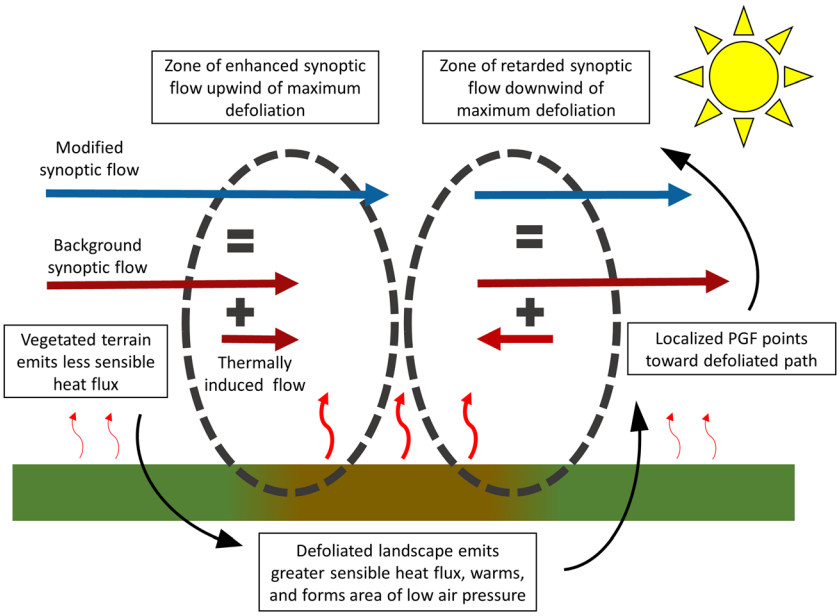

Fig. 8 Shematic illustrating proposed mechanisms leading to the 10-m wind speed deviations in the defoliated simulation shown in Fig. 7a

on days with large convective inhibition. However, previous work suggests that the development of a thermal gradient may be dependent on soil moisture. Barr et al. (2012) identified latent heat flux, rather than sensible heat flux, increases following Hurricane Wilma-related defoliation in a mangrove forest with corresponding high soil moisture.

The hypothesized downwind precipitation enhancement (Fig. 9) is mirrored by studies that have investigated the urban influence on warm-season precipitation. Noting the strong dependence of the urban-enhanced precipitation corridor on wind direction in Atlanta, Georgia, McLeod et al. (2017) proposed that such precipitation enhancement must necessarily be described as "flow regime dependent." Similarly, in an idealized modeling experiment of convection initiation over heated terrain, Kirshbaum (2010) showed that nascent updrafts were transported downwind according to the background flow with the area of highest hydrometeor concentration at the surface displaced from the initial position of the shallow thermal. Miller et al. (2015) drew upon this finding when comparing lightning activity over preferentially heated terrain. Though the greatest lightning frequencies occurred over eastward-oriented, sloped ridge faces, it was unclear whether this location corresponded to the point of convection initiation or if thunderstorms initiated along the ridgeline and were transported eastward by the prevailing wind.

5 Summary and conclusions

The 2017 and 2018 Atlantic hurricane seasons were grave reminders of the dangers posed by powerful tropical cyclones to residents of the US, Central American, and Caribbean

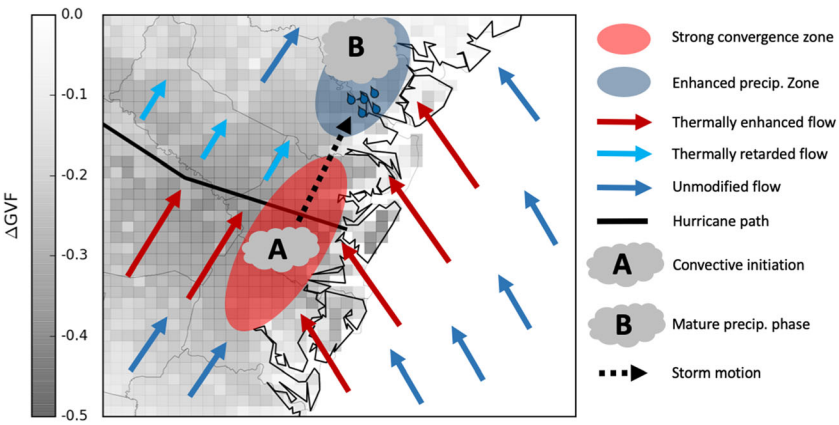

Fig. 9 Hypothesized convergence zones leading to precipitation enhancement down wind of defoliated zone (Fig. 6)

coastlines. Excess mortality estimates for Hurricane Maria in Puerto Rico alone include 1085 (Santos-Lozada and Howard 2018), 2975 (Milken Institute School of Public Health 2018), and 4645 deaths (Kishore et al. 2018). In addition to acute impacts from high wind, heavy rainfall, and storm surge inundation, several 2017 and 2018 landfalling hurricanes left more persistent scars upon their afflicted landscapes via catastrophic defoliation. Beyond damaging the intrinsic beauty of these landscapes, widespread defoliation perturbs the surface energy budget by simultaneously restricting latent heat flux and increasing sensible heat flux. The purpose of this study was to determine whether the changes in surface energy fluxes could significantly redistribute precipitation in the months following a hurricane landfall. Remote sensing analyses of vegetation reduction and recovery following Hurricane Maria in Puerto Rico were adapted to the Georgia coastline. In a first-of-its-kind analysis, this landscape evolution was then assimilated into the WRF model for a 2-month period following a hypothetical landfall on 1 June 2017. In addition to the normal vegetation and Maria-derived defoliation simulations, three additional experiments with progressively less severe defoliation were tested.

The experiment revealed that Maria-scale defoliation reduced precipitation amounts by 14% during the 30 days following the landfall within the area nearest the landfall location. Had this event occurred as modeled, the 14% reduction in June 2017 precipitation would have shifted a near-normal precipitation total for Brunswick, GA, from the 61st to the 47th percentile for the 1981–2016 period. However, on the regional scale, precipitation totals were essentially unchanged, and instead, precipitation was spatially redistributed within the domain. Using a strongly capped, quiescent synoptic day on which thunderstorm outflows did not disrupt background wind field as an archetype, the defoliation was shown to enhance 10-m wind speeds upwind of the hypothetical path and retard them downwind. Meanwhile, the sea breeze front was strengthened as onshore flow was directed more orthogonally and more strongly toward the Georgia coast. Overall, the defoliated scenario (33 days) contained two more favorable sea breeze days than the control (31 days) as determined by an application of a regional sea breeze index.

These findings hold immediate importance for emergency managers and water managers who may be unaware to account for precipitation deficits in the immediate landfall zone during disaster recovery. In addition to the near-landfall drying, another potentially even more impactful finding is that the same area of reduced precipitation was evident in the 25% Maria defoliation scenario. Thus, the defoliation following a tropical cyclone landfall may not need to be as catastrophic as Hurricane Maria to alter the water cycle in the afflicted areas. Future research should further investigate the physical processes driving the precipitation redistribution, which this study was unable to accomplish with its coarse temporal output. For instance, how is precipitation intensity altered by the reduced specific humidity over the defoliated zone? How sensitive is the precipitation redistribution to the orientation of the defoliation path? How did these processes lead to a greater percent reduction in precipitation for the 25% Maria scenario compared to the more severe defoliated landscapes? The answers to these questions will be immensely helpful when extrapolating the findings herein to future hurricane-related disasters in different locations.

Acknowledgments We thank the three anonymous reviewers whose comments strengthened the quality of this paper.

Funding information This research was supported by the Georgia Sea Grant Recovery and Response to Hurricane Irma program and the NSF Luquillo Long-Term Ecological Research Program (DEB1239764) through a sub-award from the University of Puerto Rico-Río Piedras to the University of Georgia.

References

Barr JG, Engel V, Smith TJ, Fuentes JD (2012) Hurricane disturbance and recovery of energy balance, CO2 fluxes and canopy structure in a mangrove forest of the Florida Everglades. Agric For Meteorol 153: 54–66. https://doi.org/10.1016/j.agrformet.2011.07.022

Bossak BH, Keihany SS, Welford MR, Gibney EJ (2014) Coastal Georgia is not immune: hurricane history, 1851–2012. Southeast Geogr 54:323–333

Daly C, Neilson RP, Phillips DL (1994) A statistical-topographic model for mapping climatological precipitation over mountainous terrain. J Appl Meteorol 33:140–158. https://doi.org/10.1175/1520-0450(1994)033<0140:ASTMFM>2.0.CO;2

Forrester MM, Maxwell RM, Bearup L, Gochis D (2018) Forest disturbance feedbacks from bedrock to atmosphere using coupled hydrometeorological simulations over the Rocky Mountain headwaters J Geophys Res: Atmos In press doi:https://doi.org/10.1029/2018JD028380

Frysinger JR, Lindner BL, Brueske SL (2003) A statistical sea-breeze prediction algorithm for Charleston. South Car Wea Forecast 18: 614–625. https://doi.org/10.1175/1520-0434(2003)018<0614:ASSPAF>2.0.CO;2

Garcia-Carreras L, Parker DJ, Marsham JH (2010) What is the mechanism for the modification of convective cloud distributions by land surface–induced flows? J Atmos Sci 68:619–634. https://doi.org/10.1175/2010JAS3604.1

Georgia Department of Agriculture (2018a) Georgia Agriculture Commissioner Gary W. Black issues statement on latest Georgia Forestry Commission's estimation of $762,683,909 in losses from Hurricane Michael

Georgia Department of Agriculture (2018b) Updated damage assessments from Hurricane Michael Released. http://agr.georgia.gov/updated-damage-assessments-from-hurricane-michael-released.aspx. Accessed 11 February 2019

Ghosh S, Mishra DR, Gitelson AA (2016) Long-term monitoring of biophysical characteristics of tidal wetlands in the northern Gulf of Mexico — a methodological approach using MODIS. Remote Sens Environ 173:39–58. https://doi.org/10.1016/j.rse.2015.11.015

Hu T, Smith BR (2018) The impact of Hurricane Maria on the vegetation of Dominica and Puerto Rico using multispectral remote sensing remote sensing 10 doi:https://doi.org/10.3390/rs10060827

Hu X-M, Xue M, McPherson RA (2017) The importance of soil-type contrast in modulating August precipitation distribution near the Edwards Plateau and Balcones Escarpment in Texas J Geophys Res: Atmos In press doi:https://doi.org/10.1002/2017JD027035

Kirshbaum DJ (2010) Cloud-resolving simulations of deep convection over a heated mountain. J Atmos Sci 68:361–378. https://doi.org/10.1175/2010JAS3642.1

Kishore N et al (2018) Mortality in Puerto Rico after Hurricane Maria New England Journal of Medicine 379:162-170. https://doi.org/10.1056/NEJMsa1803972

Landsea CW, Franklin JL (2013) Atlantic hurricane database uncertainty and presentation of a new database format. Mon Weather Rev 141: 3576–3592. https://doi.org/10.1175/MWR-D-12-00254.1

McLeod J, Shepherd M, Konrad CE (2017) Spatio-temporal rainfall patterns around Atlanta, Georgia and possible relationships to urban land cover. Urban Clim 21:27–42. https://doi.org/10.1016/j.uclim.2017.03.004

Midwestern Regional Cimate Center (2019) Cli-MATE Wind Rose Tool. https://mrcc.illinois.edu/CLIMATE/. Accessed 18 January 2019

Milken Institute School of Public Health (2018) Ascertainment of the estimated excess mortality from Hurricane Maria in Puerto Rico. George Washington University, Washington, D.C.

Miller PW, Ellis A, Keighton S (2015) Spatial distribution of lightning associated with low-shear thunderstorm environments in the central Appalachians region. Phys Geogr 36:127–141. https://doi.org/10.1080/02723646.2015.1011257

Miller PW, Kumar A, Mote TL, Moraes FDS, Mishra DR (2019) Persistent hydrological consequences of Hurricane Maria in Puerto Rico. Geophys Res Lett 46:1413–1422. https://doi.org/10.1029/2018GL081591

NWS (2018) Hurricane Michael Hits Georgia. https://www.weather.gov/ffc/2018_hurricane_michael. Accessed 11 February 2019

Parrotta JA, Lodge DJ (1991) Fine root dynamics in a subtropical wet forest following hurricane disturbance in Puerto Rico. Biotropica 23:343–347. https://doi.org/10.2307/2388250

Pielke, Roger A (2001) Influence of the spatial distribution of vegetation and soils on the prediction of cumulus convective rainfall. Rev Geophys 39:151–177. https://doi.org/10.1029/1999RG000072

Pieri AB, von Hardenberg J, Parodi A, Provenzale A (2015) Sensitivity of precipitation statistics to resolution, microphysics, and convective parameterization: a case study with the high-resolution WRF Climate Model over Europe. J Hydrometeorol 16:1857–1872. https://doi.org/10.1175/JHM-D-14-0221.1

Rochetin N, Couvreux F, Guichard F (2017) Morphology of breeze circulations induced by surface flux heterogeneities and their impact on convection initiation. Quart J Roy Meteorol Soc 143:463–478. https://doi.org/10.1002/qj.2935

Santos-Lozada AR, Howard JT (2018) Use of death counts from vital statistics to calculate excess deaths in puerto rico following Hurricane Maria JAMA In press doi:https://doi.org/10.1001/jama.2018.10929

Scatena FN, Larsen MC (1991) Physical aspects of Hurricane Hugo in Puerto Rico. Biotropica 23:317–323. https://doi.org/10.2307/2388247

Schwartz CS et al (2009) Next-day convection-allowing WRF model guidance: a second look at 2-km versus 4-km grid spacing. Mon Weather Rev 137:3351–3372. https://doi.org/10.1175/2009MWR2924.1

Shem W, Shepherd M (2009) On the impact of urbanization on summertime thunderstorms in Atlanta: Two numerical model case studies. Atmos Res 92:172–189. https://doi.org/10.1016/j.atmosres.2008.09.013

Shepherd JM, Carter M, Manyin M, Messen D, Burian S (2010) The impact of urbanization on current and future coastal precipitation: a case study for Houston Environment and Planning B. Plan Des 37: 284–304. https://doi.org/10.1068/b34102t

Sims AP, Raman S (2016) Interaction between two distinct mesoscale circulations during summer in the coastal region of eastern USA. Bound-Layer Meteorol 160:113–132. https://doi.org/10.1007/s10546-015-0125-6

Skamarock WC, Klemp JB (2008) A time-split nonhydrostatic atmospheric model for weather research and forecasting applications. J Comput Phys 227:3465–3485. https://doi.org/10.1016/j.jcp.2007.01.037

UCAR (2017) User's guides for the advanced research WRF (ARW) Modeling System, Version 3. http://www2.mmm.ucar.edu/wrf/users/docs/user_guide_V3.9/ARWUsersGuideV3.9.pdf. Accessed 9 May 2017

Wang Y, Tang J, Matyas C (2016) Simulating effects of land surface characters on tropical cyclone rainfall pattern using Hurricane Nature Run (HNR) and Weather Research and Forecasting (WRF) Model. Paper presented at the 32nd Conference on Hurricanes and Tropical Meteorology, San Juan, PR, 17–22 April 2016

Wang Y, Geerts B, Liu C (2018) A 30-year convection-permitting regional climate simulation over the interior western United States. Part I: Validation. Int J Climatol 38:3684–3704. https://doi.org/10.1002/joc.5527

Woolbright LL (1991) The impact of Hurricane Hugo on forest frogs in Puerto Rico. Biotropica 23:462–467. https://doi.org/10.2307/2388267

Zaitchik BF, Santanello JA, Kumar SV, Peters-Lidard CD (2012) Representation of soil moisture feedbacks during drought in NASA Unified WRF (NU-WRF). J Hydrometeorol 14:360–367. https://doi.org/10.1175/JHM-D-12-069.1